

Who Make Drivers Stop? Towards Driver-centric Risk Assessment: Risk Object Identification via Causal Inference

Chengxi Li¹ Stanley H. Chan¹ Yi-Ting Chen²

Abstract—We propose a framework based on causal inference for risk object identification, an essential task towards driver-centric risk assessment. In this work, risk objects are defined as objects influencing driver’s goal-oriented behavior. There are two limitations of the existing approaches. First, they require strong supervisions such as risk object location or human gaze location. Second, there is no explicit reasoning stage for identifying risk object. To address these issues, the task of identifying causes of driver behavioral change is formalized in the language of functional causal models and interventions. Specifically, we iteratively simulate causal effect by removing an object using the proposed driving model. The risk object is determined as the one causing the most substantial causal effect. We evaluate the proposed framework on the Honda Research Institute Driving Dataset (HDD). The dataset provides the annotation for risk object localization to enable systematic benchmarking with existing approaches. Our framework demonstrates a substantial average performance boost over a strong baseline by 7.5%.

I. INTRODUCTION

In this paper, we tackle the problem of risk object identification, an essential step towards driver-centric risk assessment. Human drivers have the ability to identify risk objects and assess their risk in order to drive safely. Note that risk objects are defined as objects influencing drivers goal-oriented behavior. For instance, while turning left at an intersection, a driver is able to efficiently attend to relevant objects (e.g., oncoming vehicles, crossing pedestrians, construction zones, and so on), assess their risk, and decide if they should stop or yield. We believe understanding human drivers’ decision making processes is crucial towards intelligent automated driving systems.

To achieve the ultimate goal, existing works for risk object identification can be categorized into two families. First, supervised learning-based algorithms are trained to regress risk objects’ location or to generate drivers’ attention maps. Specifically, in [38], [8], [26], the risk object identification task is formulated as an object detection problem. Alternatively, the task can be treated as pixel-level drivers attention prediction by mimicking human gaze behavior [2], [34], [31]. While favorable results have been shown, labeling risk objects using bounding boxes and human gaze behavior is noisy and time-consuming.

C. Li¹ and S. H. Chan¹ are with Department of Electrical and Computer Engineering, Purdue University, West Lafayette, IN, USA. Y.-T. Chen² is with Honda Research Institute USA, San Jose, CA, USA.

The work was done when C. Li was an intern at Honda Research Institute, USA.

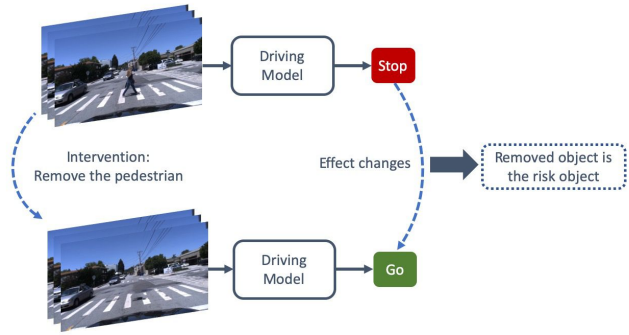


Fig. 1: Causal inference for risk object identification. Intervening the input by removing the pedestrian changes driver behavior (effect) from ‘stop’ to ‘go’, indicating the removed object is the risk object (cause) for ‘stop’.

The second family is by selecting regions/objects with high activation in visual attention heat maps learned from end-to-end driving models with explicit attention mechanisms [15], [32]. Kim and Canny [15] proposed a two-stage framework. In the first stage, a visual attention mechanism is embedded in a end-to-end trainable driving model (i.e., from images to steering angle and velocity). The attention model highlights image regions that potentially influence the networks output. To remove false influences estimated in the first stage, a causal filtering step as the second stage is applied to determine which input regions actually influence the network’s behavior. Wang et al. [32] extends pixel-level attention [15] with object-level attention by introducing a taxonomy of objectness representations. The pixel- and object-level attention modeling are trained purely by task-driven objective functions. There is no guarantee if networks will attend on relevant regions/objects that influence drivers’ tactical behavior. Note that a related issue “causal misidentification” has been raised in training end-to-end driving models [7].

In this paper, we propose a novel two-stage framework to tackle aforementioned limitations. The task of identifying causes of driver behavioral change is formalized in the language of functional causal models (FCM) and interventions [25]. Figure 1 depicts the concept of intervention for risk object identification. To realize the concept, we first train the proposed driving model that is able to manipulate at an object level. Specifically, given an image, it is intervened

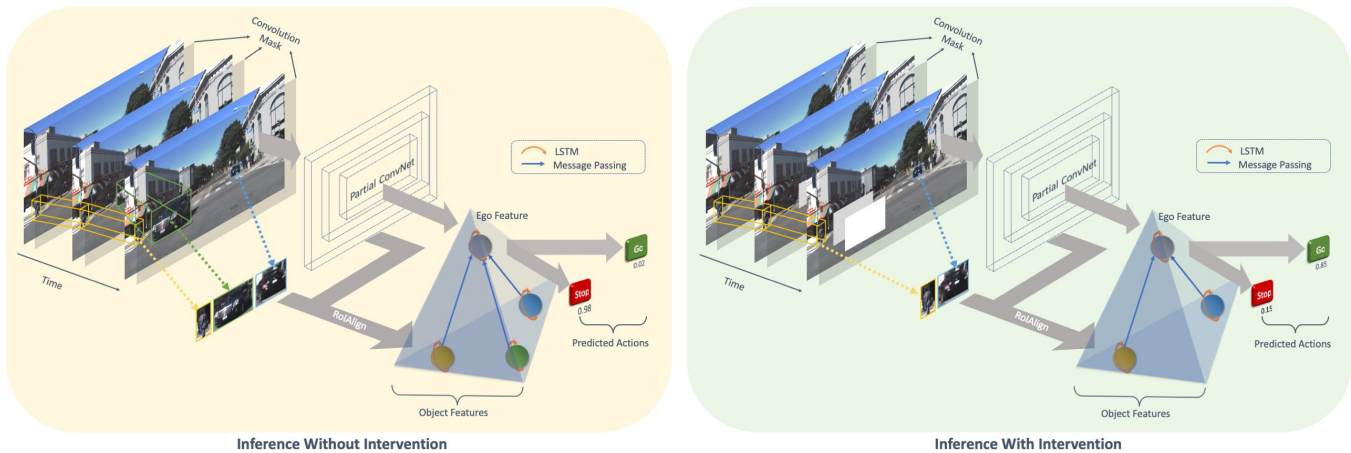


Fig. 2: An overview of our framework. The right and left figures show the inference process with and without intervention, respectively. Both employ the same driving model to output the predicted driver action. The inputs to the driving model include a sequence of RGB frames, a sequence of binary masks and object tracklets. Partial convolution and average pooling are employed to obtain the ego features while object features are extracted by RoIAlign. Each feature is modeled temporally and then propagates information to form a visual representation of the scene for final prediction. On the right, the input is intervened at an object level by masking out the selected object on the convolution mask and also removing it from the tracklets. For example, we remove the car in the green box and the driving model returns a high confidence score of ‘go’.

by removing a specific object. The driving model is learned to predict the corresponding action in the absence of the object guided by a proposed training strategy. Note that the causes of driver behavioral change are assumed to be traffic participants (i.e., vehicle and pedestrian) to simplify the problem scope. At the second stage, we iteratively simulate the causal effect by removing an object using the trained driving model. The risk object is determined by the one causing the most substantial causal effect.

Note that the proposed framework requires minimal annotations in comparison with the methods discussed in the first family. The proposed framework requires drivers’ tactical behavior labels (e.g., go, stop, straight, left turn, and right turn) at video frame level instead of labeling important object location in every frame [8]. Furthermore, it is less noisy to determine tactical behaviors than to process human gaze behaviors [2], [34].

We validate the proposed framework on Honda Research Institute Driving Dataset (HDD) [27]. The experimental results show that the proposed framework achieves favorable performance both quantitatively and qualitatively. Note that a 7.5 percent average performance boost is obtained over a strong baseline [15]. Furthermore, extensive ablation studies are conducted to justify our design choices.

II. RELATED WORK

A. Risk Assessment

To survive, the living agents have the ability to assess risk for decision making. Lefèvre et al. [19] survey existing methods for motion prediction and risk assessment for intelligent vehicles. The underlying risk assessment methodology is to predict all the possible future trajectories of all the vehicles in the scene and check for collisions. While

mainstream studies follow “trajectory prediction + collision check”, Lefèvre et al. [18] define the computation of risk to be the probability that expectation and intention do not match. While the paradigm relates to the proposed definition of risk objects, i.e., objects influencing drivers goal-oriented behavior, the underlying risk object identification process is different. In [18], a risk object is identified by computing the “hazard probability” (based on the proposed computation of risk) of vehicles via inference in a learned dynamic Bayesian network. We identify the risk object by simulating the causal effect via removing an object using the trained driving model.

B. Causal Confusion in End-to-end Driving Models

Recent successes [4], [35] demonstrate that a driving policy can be learned via a supervised manner from human demonstration [5], [32], [16]. Additionally, recent driving datasets [27], [37] with high quality drivers’ demonstration enable training driving models under different real-world scenarios. However, the issue of causal confusion in training end-to-end driving models has been discussed in [6], [10], [7]. Haan et al. [7] propose to incorporate the concept of functional causal models [25] into imitation learning to address the issue of “causal misidentification. In [10], they do not estimate the causal structure but overcome the causal misidentification issue by adding noises to inputs.

Our work is complementary to [10], [7]. Specifically, the focus of [10], [7] is to improve the robustness of driving models. Instead, our proposed driving model is to enable intervention for risk object identification. We believe the two lines of works should be studied jointly to obtain robust driving models with explicit reasoning mechanisms.

III. METHOD

A. Functional Causal Model and Intervention

We use Y to denote an effect variable and $X := \{X_1, X_2, \dots, X_n\}$ indicates a set of potential cause variables that may affect Y . A directed acyclic graph (DAG) is used to represent causal relationships by arrows between the variables, pointing from causes to the effect. A functional causal model (FCM) represents the effect variable Y as a function with parameter ϕ , i.e., $Y = f_\phi(\text{Pa}(Y), E)$. $\text{Pa}(Y)$ denotes parent nodes of Y , corresponding to its direct causes, and it is a subset of X . E is independent of X . An intervention $do(X_i)$ changes variable X_i 's states and leads to the change in Y if $X_i \in \text{Pa}(Y)$.

In our setting, the effect Y is defined as the driver's tactical behavior which can potentially be affected by a set of objects (cause variables X). In classic FCM, cause variables are summarized to be pre-defined concepts with each X_i having specific semantics (e.g., age, height and weight), thus $\text{Pa}(Y)$ is determined upon Y . However, the cause variables in our settings do not correspond to fixed concepts and the number of objects varies, resulting a changeable $\text{Pa}(Y)$ in different scenes. Thus, we propose a driving model, served as an approximated FCM $Y = f_\phi(X, E)$, which takes every X_i into account and parameterizes with neural network parameters ϕ to implicitly model the direct cause $\text{Pa}(Y)$.

In causal inference, we iteratively intervene the inputs to the driving model by removing each object, $do(X_i) := X - \{X_i\}$. We observe the changes in effect $Y_{do(X_i)} = f_\phi(X - \{X_i\}, E)$ and determine the risk object to be the one causing the most substantial effect changes.

In the following sections, we discuss the steps to realize the language of FCM and interventions for risk object identification.

B. Object-level Manipulable Driving Model

An overview of the driving model architecture is visualized in Fig. 2. Given video frames, we utilize Partial Convolution Networks [22], [23] and average pooling to represent features of the ego vehicle. Partial convolution operation is first introduced in the image inpainting application where this masked and re-normalized convolution operation enables the hallucination in the masked area because convolutional results depend only on the non-masked regions at every layer. The operation enables removing objects for intervention.

A partial convolutional layer requires two inputs, i.e., a RGB frame and corresponding one-channel binary mask. The pixel value of a mask is set to be 1 by default. In Section III-C and III-D, the pixels of the selected object is set to be 0 for training driving models and interventions. To obtain object-level representation, we apply Mask R-CNN [11] and Deep SORT [33] to detect and track every object throughout time. RoIAlign [11] is employed to extract object representations. At time t , the ego vehicle features and object features are updated via long short-term memory (LSTM) module [12]. This temporal modeling process captures the dynamics of ego vehicle and objects.

Motivated by [32], [20], both pixel-level and object-level features are essential for driving scene tasks. Hence, we aggregate the two sources of features via message passing.

$$g = h_e \oplus \frac{1}{N} \left(\sum_{i=1}^N h_i \right) \quad (1)$$

where g is defined as the aggregated features, h_e represents the ego's features obtained after temporal modeling and $h_o = \{h_1, h_2, \dots, h_N\}$ are the N object features. \oplus indicates a concatenation operation. To manipulate the representation at an object level, we set the value to be 0 at the location of the selected object. The mask influences the features extracted from partial convolution and disconnects the message of the selected object from the rest. In the end, this representation g is passed through fully connected layers to obtain the final classification of the driver behavior. For our purpose to study risk object identification, we categorize the driver behavior to be either 'go' or 'stop'.

C. Training with Intervention

We cluster and label the training samples into two categories (1) 'GO': the ego vehicle moves without stopping and (2) 'STOP': the ego vehicle stops or yields for something. This is the only supervision signal that we use in the training stage. As we know, driving models can be improved by training on samples with different traffic configurations. Due to the limited real-world human driver demonstrations, we design a training strategy and borrow the concept of intervention from causal inference studies [25] to improve the robustness of the driving model. We generate new configurations by following a simple logic that the removal of non-causal object does not affect the behavior of the ego vehicle. For instance, in the 'GO' scenario, the ego vehicle goes straight and passes an intersection, removing a pedestrian walking on the sidewalk will not influence the behavior of the ego vehicle.

In category (1), it is fine to discard any object without influencing ego vehicle behavior. However, the same strategy is not applicable to category (2) because we need to know the causal object in order to remove non-casual objects. This requires intensive labeling of risk object localization. Note that this contradicts to the spirit of the proposed risk object identification framework. Moreover, even if the annotations of causal object is given, we cannot intervene on the causal object and simply change the driver behavior to 'GO'. This is because traffic situations are inherently complicated, making the intervened driver behavior unclear. For instance, imagine that under a congestion circumstance where the ego vehicle stops for the front vehicle at an intersection, while the traffic light shows red. In such case, the front car is labeled as the risk object (cause). However, removing the front car does not necessarily lead the ego vehicle from stop to go because there is a red light.

Algorithm 1 provides the pseudo-code of the proposed training process. For training samples in category (1), we randomly select one object k to intervene. Based on the

Algorithm 1: Training Driving Model with Intervention

T : Number of frames
 N : Number of objects in the given tracklet list
 h_e : Hidden states of ego in LSTM module
 h_o : Hidden states of objects in LSTM Module $h_o := \{h_1, h_2, \dots, h_N\}$
A: Ground truth driver behavior (either ‘GO’ or ‘STOP’)
Input: A sequence of RGB frames $I := \{I_1, I_2, \dots, I_T\}$
Output: Confidence score of driver behaviors s^{go}, s^{stop}

```

1:  $O := \text{DetectionAndTracking}(I)$ 
    $:= \{O_1, O_2, \dots, O_N\}$  // List of tracklets
2: if A is ‘GO’ and  $N > 1$  then
3:   // Randomly choose one object to remove
    $k := \text{RandomSelect}(N)$ 
4: else
5:    $k$  is empty
6: end if
7: // Mask out the region of object  $k$  on each mask frame
    $M := \text{MaskGenerator}(I, O_k)$ 
8: // Remove the object  $k$  from the tracklet list
    $O' = O - \{O_k\}$ 
9:  $s^{go}, s^{stop} := \text{DrivingModel}(I, M, O')$  //Defined as
   below
10: return  $s^{go}, s^{stop}$ 

```

```

1: function DRIVINGMODEL( $I, M, O$ )
2:   for  $t \in \{1, 2, \dots, T\}$  do
3:      $e_t := \text{EgoFeature}(I_t, M_t)$ 
4:      $h_e := \text{LSTM}(e_t, h_e)$ 
5:     for  $O_i \in O$  do
6:        $f_i^t := \text{RoIAlign}(o_i^t)$  // Object Features ( $o_i^t$ 
   is  $i$ -th object’s bounding box at time  $t$ )
7:        $h_i := \text{LSTM}(f_i^t, h_i)$ 
8:     end for
9:   end for
10:   $g := \text{MessagePassing}(h_e, h_o)$ 
11:   $s^{go}, s^{stop} := \text{ActionClassifier}(g)$ 
12:  return  $s^{go}, s^{stop}$ 
13: end function

```

detection and tracking results, a one-channel binary mask is generated to cover the k -th object’s region to be unseen.

$$M_t(i, j) = \begin{cases} 0, & \text{if } (i, j) \text{ in region } o_k^t \\ 1, & \text{otherwise} \end{cases} \quad (2)$$

where M_t denotes the generated mask at time t , o_k^t is the bounding box of k -th object at time t and (i, j) is the pixel coordinate. This mask and the corresponding RGB frame will be the inputs to the partial convolutional layer in the driving model. Notice that k -th object is discarded from the tracklet list before feeding into the driving model.

Algorithm 2: Inference for Risk Object Identification

T : Number of frames
 N : Number of objects
Input: A sequence of RGB frames $I := \{I_1, I_2, \dots, I_T\}$
 where the ego car stops
Output: Risk object ID

```

1:  $O := \text{DetectionAndTracking}(I)$ 
    $:= \{O_1, O_2, \dots, O_N\}$  // List of tracklets
2: for  $O_k \in O$  do
3:   // Mask out the region of object  $k$  on each frame
    $M := \text{MaskGenerator}(I, O_k)$ 
4:   // Remove the object  $k$  from the tracklet list
    $O' = O - \{O_k\}$ 
5:   // Predict the action of ego car without object  $k$ 
    $s_k^{go}, s_k^{stop} := \text{DrivingModel}(I, M, O')$ 
6: end for
7: return  $\arg \max_k (s_k^{go})$ 

```

	# Training Frames	# Validation Frames	# Test Frames
Crossing Vehicle	18,696	5,652	311
Crossing Pedestrian	20,784	3,999	84
Parked Vehicle	11,484	3,537	136
Congestion	21,132	5,607	99

TABLE I: Statistics of train/val/test samples in the HDD used in our experiments.

D. Inference for Risk Object Identification

Our objective is to identify which object influences driver’s goal-oriented behavior. As explained in Algorithm 2, given the video frames and tracklets, we iterate over and intervene on each object presented in the scene. The intervened input is passed through the trained driving model which returns the predicted confidence score of two driver actions. We choose the object with the highest confidence score of ‘go’, indicating this object causes most substantial behavioral change. We select it as the predicted risk object.

IV. EXPERIMENTS

A. Dataset

We evaluate the proposed framework on the HDD dataset [27], a multisensory 104-hour naturalistic driving dataset with frame-level annotations of tactical driver behavior using a 4-layer representation. The **Stimulus-driven action** layer includes behaviors such as ‘stop’ and ‘deviate’ and **Cause** layer explains the reasons of behavioral changes. For example, while going straight, a stopped car causes the driver to stop. In total, the dataset is labeled 6 **Cause** scenarios. They are *Stopping for Congestion*, *Stopping for Crossing Vehicle*, *Deviating for Parked Vehicle*, *Stopping for Pedestrian*, *Stopping for Sign*, and *Stopping for Red Light*. Two types of movable objects (i.e., vehicle and pedestrian) and the first 4 scenarios defined in the HDD dataset are

Driving Model	Mask	Training with Intervention	Crossing Vehicle			Crossing Pedestrian			Parked Vehicle			Congestion		
			$Acc_{0.5}$	$Acc_{0.75}$	$mAcc$	$Acc_{0.5}$	$Acc_{0.75}$	$mAcc$	$Acc_{0.5}$	$Acc_{0.75}$	$mAcc$	$Acc_{0.5}$	$Acc_{0.75}$	$mAcc$
Vanilla CNN	RGB	✗	36.0	35.7	31.4	20.2	16.7	14.9	36.8	32.4	29.7	87.9	83.9	76.8
Partial CNN	RGB	✗	38.6	37.6	33.5	22.6	19.0	16.2	36.0	32.4	29.0	81.8	81.8	73.7
	RGB	✓	41.2	40.5	36.2	19.0	16.7	13.5	<u>39.0</u>	<u>36.8</u>	<u>32.4</u>	94.9	91.0	82.6
	Convolution	✗	38.6	37.6	33.6	22.6	17.9	16.2	36.8	33.1	29.5	88.9	84.8	78.0
	Convolution	✓	44.4	<u>43.1</u>	<u>38.5</u>	25.0	<u>22.6</u>	<u>19.3</u>	34.6	33.1	28.8	88.0	84.8	77.3
Partial CNN + Object	Convolution	✗	39.9	38.9	34.4	<u>27.4</u>	<u>22.6</u>	18.9	31.6	27.9	24.7	91.9	87.9	79.7
	Convolution	✓	49.2	48.6	43.0	35.7	32.1	27.0	47.1	44.9	39.8	<u>92.9</u>	<u>88.9</u>	<u>81.0</u>

TABLE II: Ablation studies. Results of risk object identification in four scenarios on the HDD. The unit is %. The best and second performances are shown in bold and underlined, respectively.

selected to study risk object identification. We utilize frame-level action label to train our driving model. The train/test data split is the same as [27].

The dataset provides annotations for risk object localization for a very small portion of the dataset, making it infeasible to train a robust supervised learning-based object detection model to regress its localization. The statistics of train/val/test samples is presented in TABLE I.

In terms of evaluation metrics, we report accuracy number of correct predictions over the number of samples. A correct prediction is defined to have an Intersection over Union (IoU) score between the selected box and the ground truth box above a threshold. Similar to [21], [39], accuracies at IoU thresholds of 0.5 and 0.75 are reported, as well as a mean accuracy $mACC$ which is calculated by averaging accuracies at 10 IoU thresholds evenly distributed from 0.5 to 0.95.

B. Implementation Details

We implemented our framework in PyTorch [1], and performed all experiments on a system with Nvidia Quadro RTX 6000 graphics cards.

The input to the framework is a sequence of frames with a resolution of 299×299 at 3 fps, and T is set to 3 in all the experiments, approximately 1s. The corresponding input mask maintains the same size as the input image. The convolutional backbone is a InceptionResnet-V2 [30], pre-trained on ImageNet [28] and modified with partial convolution operation [22], [23]. A Detectron model [9] trained on MSCOCO [21] is used to generate bounding boxes for objects. RoIAlign extracts object features with size $20 \times 8 \times 8$ from the Conv2d_7b layer, which is then padded into a 1-D vector of size 1280.

We follow the same way as [36] to initialize the hidden states with channel number set to 512 and also use dropout [29] of 0.5 at hidden state connections in LSTM module. The aggregated feature g concatenated from ego features and object features is a 1-D vector with 1024 channels. Similar to [15], the output sizes of 3 fully-connected layers before the final binary classifier are 100, 50 and 10, respectively.

The network is trained end-to-end for 10 epochs with batch size set to 16. We use Adam [17] optimizer with default parameters, learning rate 0.0005, and weight decay 0.0005.

Method	$mAcc$			
	Crossing Vehicle	Crossing Pedestrian	Parked Vehicle	Congestion
Random Selection	15.1	7.1	6.4	5.5
Driver's Attention Prediction * [34]	16.8	8.9	10.0	21.3
Object-level Attention Selector * [32]	36.5	21.2	20.1	8.9
Pixel-level Attention + Causality Test * [15]	41.9	<u>21.5</u>	<u>34.6</u>	<u>62.7</u>
Ours	43.0	27.0	39.8	81.0

TABLE III: Comparison with other risk object identification methods. The methods with * are re-implemented by us. The unit is %. The best and second performances are shown in bold and underlined, respectively.

C. Ablation Studies

We conduct ablation studies in TABLE II to provide a comprehensive understanding of the contributions for each component.

Architecture of the Driving Model. Our proposed driving model uses features from CNN features and object features. For CNN features, we test two backbone features, i.e., vanilla convolution and partial convolution.

Intervention Mask. Different from vanilla CNN, the input to partial CNN includes an extra mask, offering two options to intervene an image. We either input a RGB image with selected region masked out or feed in a binary mask with selected region set to 0 and the rest to 1. We denote the two ways of intervention as ‘RGB mask’ and ‘Convolution mask’ in TABLE II.

Training with Intervention. To discover how the framework performs, especially when using the model trained with more traffic configuration variations, we explore two experimental settings training with and without intervention. Notice that for Partial CNN model, we always use convolution mask to remove selected objects when training with intervention. In Partial CNN + Object model, we additionally remove the selected object features during message passing.

By analyzing the results, our completed framework (last row in TABLE II) boosts the $mACC$ by 11.6%, 13.5%, 11% and 7.3%, respectively, compared with the lowest accuracies. It ranks first in three scenarios (Crossing Vehicle, Crossing Pedestrian and Parked Vehicle) and second in Congestion case.

Training with intervention always leads to an increase in accuracy when the driving model is modeled with object-level information. However, it does not necessarily help

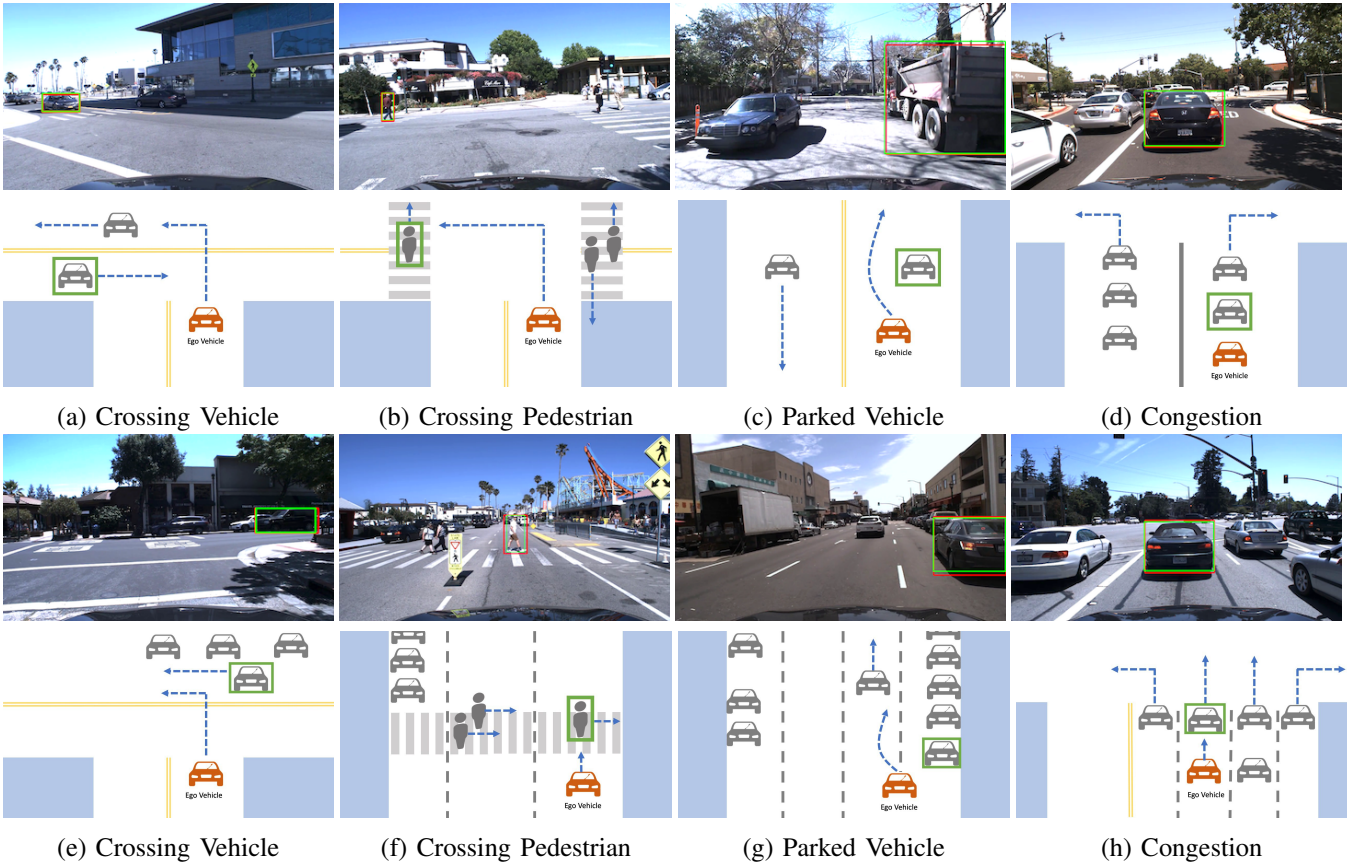


Fig. 3: Sample scenes from HDD dataset with the identified risk objects obtained from our method visualized. The top row shows an egocentric view where green boxes indicate inferred risk objects while ground truth ones are in red. A bird’s-eye-view representation is presented in the bottom row, providing information including scene layout, intentions of traffic participants. The objects in green frames are the risk objects detected by our method.

the performance when the driving model is downgraded to Partial CNN only.

In terms of intervened mask type, an interesting phenomenon is observed that in Crossing Vehicle and Crossing Pedestrian scenarios, intervening with convolution mask achieves higher accuracy than RGB mask in general. However, in the other two scenarios, this trend is no more noticeable. Our conjecture is that, when the ego vehicle deviates for parked vehicle or stops for congestion, the target risk object is pixel-wisely salient, taking up the majority area of the frame. Under such circumstance, inputting a masked RGB frame could be enough for changing the driving model output significantly. Thus, the increased performance resulting from hallucination effect of convolution mask is relatively unremarkable.

D. Quantitative Evaluation

We compare our approach with existing works for risk object identification in TABLE III.

Random Selection. We first propose a naive baseline which randomly selects one object as the risk object from all the detections for a given frame. This method does not process any visual information and we show the result to provide a basic measure of the difficulty of this task.

Driver Attention Prediction. We utilize a supervised learning model [34] to predict the driver’s heated attention maps at each frame. For every detected object, we compute the average heat value inside the object region. The risk object is chosen to be the most heated object, indicating driver’s highest attention falls into that region. The model is trained with human gaze as supervision, which is unavailable in HDD dataset. Thus, we test the model pre-trained on BDD-A dataset [34]. The performance of this method is slightly better than **Random Selection**. By visualizing the predicted attention map, we discover that the heated spots tend to cluster around the vanishing point. Note that the phenomenon has been raised in [3]. The reference highlights one of the challenges of mimicking human gaze behavior.

Object-level Attention Selector. Wang et al. [32] design an object-centric driving model by learning object-level attention weights, which can be further used as an object selector in risk object identification task. Motivated by their design, we modify the message passing in our driving model to be object-level attention and re-train our model. We evaluate the accuracy in four scenarios based on the selected object with the highest object-attention score.

Pixel-level Attention + Causality Test. Kim et al. [15] propose a causality test to search for regions that influence

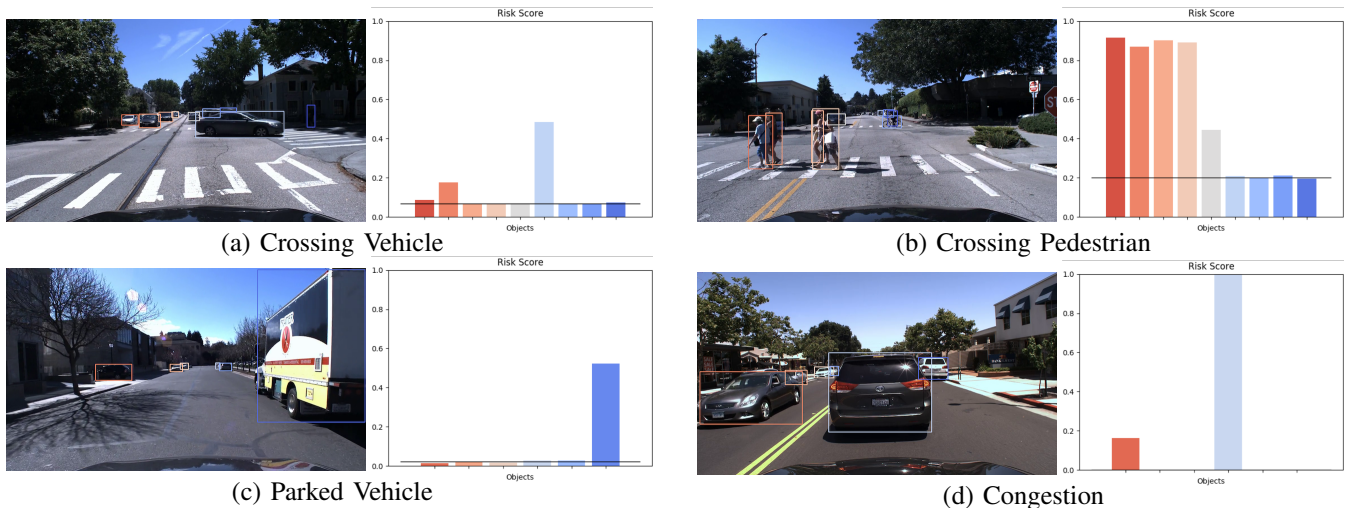


Fig. 4: Sample scenes from the HDD dataset with object risk score visualized. On the left, all detected objects are shown in bounding boxes with different colors. The risk score of each object is depicted in a bar chart on the right. The color of each bar is one-to-one matched to the bounding box. We use a black horizontal line to indicate the predicted ‘go’ score of the ego vehicle without applying any intervention.

the network’s output behavior. They utilize the pixel-level attention map learned in the driving model to sample particles conditioned on the attention value over an input image. The sampled particles are clustered to further produce a convex hull to form region proposals. Each convex hull is masked out on a RGB image, and the image is sent to the trained driving model to perform a causality test, iteratively. The region which leads to the maximum decrease of prediction performance will be the risk object. For a fair comparison, we replace the region proposals with object detections and utilize the pixel-level attention to filter out detections with low attention values. In the experiments, we set the threshold at 0.002.

The reason of this modification is that, compared with our detections generated from the state-of-the-art object detection algorithm, the region proposals obtained from pixel-level attention are not guaranteed to be an object entity, which results in an extremely low IoU and accuracy. Note that the code of obtaining region proposals is not public available. The performance of this method is reported in the third row of TABLE III, which is the closest to our results since the causality test is similar to our inference with intervention. Our performance is better because our driving model is manipulable at an object-level and it is trained with intervention strategy for robustness.

E. Visualization

Apart from quantitative evaluation, we demonstrate the capability of our method by visualizing examples of the four scenarios in Fig. 3 and Fig. 4.

In Fig. 3, ground truth risk objects are enclosed in red bounding boxes and our inferred results are shown in green. For a better representation of the interactions among traffic participants, we provide a birds-eye-view (BEV) pictorial illustration in the second row. This BEV figure depicts the

scene layout, the ego vehicle’s intention, as well as other traffic participants’, and the identified risk object in the green box. In Fig. 3 (b), three pedestrians are presented in the scene, crossing the road and moving towards different directions. Our approach correctly tags the left pedestrian to be the risk object as the ego vehicle intends to take a left turn, indicating that our driving model can potentially anticipate the ego vehicle’s intention based on historical observations.

In addition to select only one risk object, our framework is also feasible to assess the risk of every object in the scene. We visualize the results in Fig. 4 and the ego vehicles in the samples are supposed to take a ‘stop’ action. All detected objects are encased in bounding boxes with different colors, and their risk scores are in a bar chart with corresponding color. The risk score of an object is equivalent to the predicted confidence score of ‘go’ action after removing it. A higher score of ‘go’ action means a higher possibility that it is the object that stops the ego vehicle. We use a black horizontal line to indicate the predicted confidence score of ‘go’ action when the input is not intervened. If the score is less than 0.5, then the sample is classified as ‘stop’. As we see in the figures, our framework generates a reasonable risk assessment result.

F. Failure Cases

While our model shows the possibility to identify the intention of the ego vehicle based on the past motion (Fig. 3 (b)), there are situations that our driving model is confused and induce an incorrect risk object when the changes of historical motion are not obvious. In Fig. 5 (a), the ego vehicle plans to take a right turn and stops for the vehicle in the red box. However, our framework selects the white pickup truck over the black vehicle as the risk object. The reason could be the intention of the ego vehicle is ambiguous and historical cues are not informative. Additionally, in Fig. 5



Fig. 5: Examples of failure cases. Our prediction is in green and ground truth is in red.

(b), our driving model is not able to distinguish which vehicle will move first at a 4-way stop intersection and where it is going, resulting in a wrong selection. Hence, we believe explicitly modeling the ego’s intention, as well as other participants’, in the driving model will render better inference results.

V. CONCLUSIONS

In this paper, we propose a framework to identify risk objects from a causal inference perspective. Specifically, we iteratively simulate the causal effect using the proposed driving model by removing an object. The risk object is determined as the one causing the most substantial causal effect. The proposed framework demonstrates favorable quantitative performance on the HDD dataset over existing approaches. Extensive quantitative and qualitative evaluations demonstrate the feasibility to use driving model to reason causal effects. For future works, as highlighted in IV-F, explicit intention modeling of ego vehicle and other traffic participants’ will be beneficial. Furthermore, it will be valuable for practical purposes to formulate the framework into a single-stage framework as presented in [14], [24], [13], [7].

REFERENCES

- [1] PyTorch. <https://pytorch.org/>. 5
- [2] S. Alletto, A. Palazzi, F. Solera, S. Calderara, and R. Cucchiara. DR(eye)VE: A Dataset for Attention-based Tasks with Applications to Autonomous and Assisted Driving. In *CVPRW*, 2016. 1, 2
- [3] S. M. Ashish Tawari, Praneeta Mallela. Learning to Attend to Salient Targets in Driving Videos using Fully Convolutional RNN. In *ITSC*, 2018. 6
- [4] M. Bojarski, D. D. Testa, D. Dworakowski, B. Firner, B. Flepp, P. Goyal, L. D. Jackel, M. Monfort, U. Muller, J. Zhang, X. Zhang, J. Zhao, and K. Zieba. End to End Learning for Self-Driving Cars. In *arXiv preprint arXiv:1604.07316*, 2016. 2
- [5] F. Codevilla, M. Müller, A. López, V. Koltun, and A. Dosovitskiy. End-to-end Driving via Conditional Imitation Learning. In *ICRA*, 2018. 2
- [6] F. Codevilla, E. Santana, A. López, and A. Gaidon. Exploring the Limitations of Behavior Cloning for Autonomous Driving. In *arXiv preprint arXiv:1904.08980*, 2019. 2
- [7] P. de Haan, D. Jayaraman, and S. Levine. Causal Confusion in Imitation Learning. In *NeurIPS*, 2019. 1, 2, 8
- [8] M. Gao, A. Tawari, and S. Martin. Goal-oriented Object Importance Estimation in On-road Driving Videos. In *ICRA*, 2019. 1, 2
- [9] R. Girshick, I. Radosavovic, G. Gkioxari, P. Dollár, and K. He. Detectron. <https://github.com/facebookresearch/detectron>, 2018. 5
- [10] J. Hawke, R. Shen, C. Gurau, S. Sharma, D. Reda, N. Nikolov, P. Mazur, S. Micklethwaite, N. Griffiths, A. Shah, and A. Kendall. Urban Driving with Conditional Imitation Learning. In *arXiv preprint arXiv:1912.00177*, 2019. 2
- [11] K. He, G. Gkioxari, P. Dollar, and R. Girshick. Mask R-CNN. In *CVPR*, 2017. 3
- [12] S. Hochreiter and J. Schmidhuber. Long Short-term Memory. *Neural computation*, 1997. 3
- [13] T. Jayram, T. Kornuta, V. Albouy, E. Sevgen, and A. Ozcan. Learning Multi-Step Spatio-Temporal Reasoning with Selective Attention Memory Network. In *NeurIPS*, 2019. 8
- [14] N. R. Ke, O. Bilaniuk, A. Goyal, S. Bauer, H. Larochelle, C. Pal, and Y. Bengio. Learning Neural Causal Models from Unknown Interventions. In *arXiv preprint arXiv:1910.01075*, 2019. 8
- [15] J. Kim and J. Canny. Interpretable Learning for Self-driving Cars by Visualizing Causal Attention. In *ICCV*, 2017. 1, 2, 5, 6
- [16] J. Kim, T. Misu, Y.-T. Chen, A. Tawari, and J. Canny. Grounding Human-to-vehicle Advice for Self-driving Vehicles. In *CVPR*, 2019. 2
- [17] D. P. Kingma and J. Ba. Adam: A Method for Stochastic Optimization. In *arXiv preprint arXiv:1412.6980*, 2014. 5
- [18] S. Lefèvre, C. Laugier, and J. Ibañez-Guzmán. Evaluating Risk at Road Intersections by Detecting Conflicting Intentions. In *IROS*, 2012. 2
- [19] S. Lefèvre, D. Vasquez, and C. Laugier. A Survey on Motion Prediction and Risk Assessment for Intelligent Vehicles. *ROBOMECH Journal*, 1:1, 2014. 2
- [20] C. Li, Y. Meng, S. H. Chan, and Y.-T. Chen. Learning 3D-aware Egocentric Spatial-Temporal Interaction via Graph Convolutional Networks. In *ICRA*, 2020. 3
- [21] T.-Y. Lin, M. Maire, S. Belongie, J. Hays, P. Perona, D. Ramanan, P. Dollár, and C. L. Zitnick. Microsoft COCO: Common Objects in Context. In *ECCV*, 2014. 5
- [22] G. Liu, a. K. J. S. Fitsum A. Reda, T.-C. Wang, A. Tao, and B. Catanzaro. Image Inpainting for Irregular Holes using Partial Convolutions. In *ECCV*, 2018. 3, 5
- [23] G. Liu, K. J. Shih, T.-C. Wang, F. A. Reda, K. Sapra, Z. Yu, A. Tao, and B. Catanzaro. Partial Convolution based Padding. *arXiv preprint arXiv:1811.11718*, 2018. 3, 5
- [24] S. Nair, Y. Zhu, S. Savarese, and L. Fei-Fei. Causal Induction from Visual Observations for Goal Directed Tasks. In *NeurIPS 2019 Workshop on Causal Machine Learning*, 2019. 8
- [25] J. Pearl. Causality. *Cambridge University Press*, 2009. 1, 2, 3
- [26] A. Rahimpour, S. Martin, A. Tawari, and H. Qi. Context Aware Road-user Importance Estimation (iCARE). In *IV*, 2019. 1
- [27] V. Ramanishka, Y.-T. Chen, T. Misu, and K. Saenko. Toward Driving Scene Understanding: A Dataset for Learning Driver Behavior and Causal Reasoning. In *CVPR*, 2018. 2, 4, 5
- [28] O. Russakovsky, J. Deng, H. Su, J. Krause, S. Satheesh, S. Ma, Z. Huang, A. Karpathy, A. Khosla, M. Bernstein, A. C. Berg, and L. Fei-Fei. ImageNet LargeScale Visual Recognition Challenge. In *IJCV*, 2015. 5
- [29] N. Srivastava, G. Hinton, A. Krizhevsky, I. Sutskever, and R. Salakhutdinov. Dropout: A Simple Way to Prevent Neural Networks from Overfitting. *JMLR*, 2014. 5
- [30] C. Szegedy, S. Ioffe, V. Vanhoucke, and A. A. Alem. Inception-v4, Inception-ResNet and the Impact of Residual Connections on Learning. In *AAAI*, 2017. 5
- [31] A. Tawari, P. Mallela, and S. Martin. Learning to Attend to Salient Targets in Driving Videos using Fully Convolutional RNN. In *ITSC*, 2018. 1
- [32] D. Wang, C. Devin, Q.-Z. Cai, F. Yu, and T. Darrell. Deep Object Centric Policies for Autonomous Driving. In *ICRA*, 2019. 1, 2, 3, 5, 6
- [33] N. Wojke, A. Bewley, and D. Paulus. Simple Online and Realtime Tracking with a Deep Association Metric. In *ICIP*, 2017. 3
- [34] Y. Xia, D. Zhang, J. Kim, and D. W. Ken Nakayama, Karl Zipser. Predicting Driver Attention in Critical Situations. In *ACCV*, 2018. 1, 2, 5, 6
- [35] H. Xu, Y. Gao, F. Yu, and T. Darrell. End-to-end Learning of Driving Models from Large-scale Video Datasets. In *CVPR*, 2017. 2
- [36] M. Xu, M. Gao, Y.-T. Chen, L. Davis, and D. Crandall. Temporal Recurrent Networks for Online Action Detection. In *ICCV*, 2019. 5
- [37] F. Yu, W. Xian, Y. Chen, F. Liu, M. Liao, V. Madhavan, and T. Darrell. BDD100K: A Diverse Driving Video Database with Scalable Annotation Tooling. In *arXiv preprint arXiv:1805.04687*, 2018. 2
- [38] K.-H. Zeng, S.-H. Chou, F.-H. Chan, J. C. Niebles, and M. Sun. Agent-Centric Risk Assessment: Accident Anticipation and Risky Region Localization. In *CVPR*, 2017. 1
- [39] Z. Zhang, C. Yu, and D. Crandall. A Self Validation Network for Object-Level Human Attention Estimation. In *NeurIPS*, 2019. 5